Highly Stretchable and Ionically Conductive Membranes with Semi-Interpenetrating Network Architecture for Truly All-Solid-State Microactuators and Microsensors

Frédéric Braz Ribeiro, Bin Ni, Giao Nguyen, Eric Cattan, Alexander Shaplov, Frederic Vidal, Cédric Plesse

ADVANCED MATERIALS INTERFACES
Open Access
www.advmatinterfaces.de

Highly Stretchable and Ionically Conductive Membranes with Semi-Interpenetrating Network Architecture for Truly All-Solid-State Microactuators and Microsensors

*Frédéric Braz Ribeiro, Bin Ni, Giao T. M. Nguyen, Eric Cattan, Alexander S. Shaplov, Frédéric Vidal, and Cédric Plesse**

Polymeric ionic liquids (PILs) are an emerging class of materials which have attracted considerable attention as solid-state electrolytes because they combine the attractive properties of ionic liquids with the mechanical features of polymers. This paper presents a new method for the synthesis and characterization of stretchable and highly ionically conducting membranes and their subsequent use in truly all-solid-state, flexible, and soft electroactive devices. Linear conductive PIL and reinforcing poly(ethylene oxide) (PEO) network are first intimately entangled during the synthesis of a semi-interpenetrating polymer network (semi-IPN). Polymerization kinetics, thermomechanical properties, as well as ionic conductivity measurements reveal that for the 60:40 wt ratio of PEO:PIL a true synergy of the properties of both polymer partners is achieved, with ionic conductivities up to 8.7×10^{-5} S cm^{-1} at 30 °C and elongations at break greater than 100%, being both superior to each partners taken separately. The performances of these semi-IPNs as central membranes in all-solid-state electrochemical microdevices, composed of three self-supported and flexible layers, namely poly(3,4-ethylenedioxythiophene):poly(styrene sulfonate) (PEDOT:PSS)/semi-IPN membrane/PEDOT:PSS, are successfully demonstrated. Their testing as liquid-free ionic actuators and liquid-free piezoionic sensors undoubtfully proves that electromechanical and mechanoelectrical responses of these all-solid-state microdevices can reach performances identical to that of "classical" ionic liquid-filled systems.

1. Introduction

Recent developments in the field of soft robotics and wearables have stimulated the efforts toward the fabrication soft and stretchable ionic systems able to store electrochemical energy or to act as electromechanical transducers such as artificial muscles or sensors.[1,2] This trend is accelerated by the fast rise of the ionotronics which, as a change of paradigm, uses the ions of soft ionic conductors as charge carriers instead of the electrons from stiff and brittle materials.[3–5] Consequently the development of soft materials combining both high ionic conductivity and stretchability enabled transparent and stretchable ionic devices. However, liquid electrolytes contained in such functional devices tend to evaporate, sweat out or leak out and result now in a pressing demand of liquid-free truly all-solid-state ionic systems. Polymeric ionic liquids (PILs), also referred as polymerized ionic liquids or poly(ionic liquids), are probably the most promising candidates to develop liquid-free ionoelastomers.[5,6] PILs are a sub-class of polyelectrolytes in which either anions or cations are fixed to the polymer backbone while the counterions remain mobile without the addition of a liquid phase thanks to the highly dissociated nature of their ionic liquid-like structures.[7,8] They combine the inherent properties of ionic liquids such as their thermal and chemical stability as well as their high ionic conductivity, with the specific properties of polymers such as membrane elaboration and processing ability. These unique combination

F. Braz Ribeiro, B. Ni, G. T. M. Nguyen, F. Vidal, C. Plesse
CY Cergy Paris Université - LPPI
5 mail Gay Lussac, Cergy-Pontoise Cedex F-95031, France
E-mail: cedric.plesse@cyu.fr

The ORCID identification number(s) for the author(s) of this article can be found under https://doi.org/10.1002/admi.202202381.

DOI: 10.1002/admi.202202381

E. Cattan
Université de Valenciennes
CNRS
Université de Lille
YNCREA
Centrale Lille
UMR 8520—IEMN, DOAE, Valenciennes F-59313, France

A. S. Shaplov
Luxembourg Institute of Science and Technology (LIST) - Functional Polymers Team
5 Avenue des Hauts-Fourneaux, Esch-sur-Alzette L-4362, Luxembourg

of properties allowed for application of PILs in various electrochemical devices such as supercapacitors,[9,10] Li batteries,[11,12] thin film transistors,[13,14] solar cells,[15] actuators,[15–17] etc.

The physico–chemical properties of PILs are affected at the same time by the chemical structure i) of the main chain, ii) of the side chains, and iii) of the ionic couple.[18,19] Consequently, it is possible to adapt their structure to tailor "on demand" physico–chemical properties. Although the establishment of the relationship between the structure of a PIL and its ionic conductivity is ongoing and discussed, a few main trends have been highlighted. The ionic conductivity of PILs is generally coupled with the degree of freedom of the polymer chains.[20] The most studied parameter is the glass transition temperature (T_g), as the increase in T_g induces a decrease on ionic conductivity. Several parameters influence on the T_g of PILs such as the nature of the ion pair,[21,22] the chemical structure and the length of a spacer between the main chain and the ionic center,[7,23] or the architecture of the polymer chains.[24,25] To reach high ionic conductivity, the low T_g PIL is expected since ionic mobility is usually linked to the degree of freedom of the polymer chains in these materials. The ionic conductivity of the majority of PILs described in the literature generally ranges between 10^{-6} and 10^{-7} S cm^{-1} at 25 °C.[26] Table S1, Supporting Information, represents TOP 15 of the most conductive PILs reported to date and shows that the maximum of the ionic conductivity in anhydrous conditions for the thoroughly purified PIL reached 1.2×10^{-4} S cm^{-1} at 30 °C.

However, the properties of PIL based elastomers are usually a trade-off between ionic conduction and mechanical (viscoelastic) properties as these characteristics have an inversely interdependent relationship. Indeed, the required low T_g usually leads to viscous liquid like or cold flowing rubbery materials with high conductivity. The introduction of the crosslinks to improve the mechanical properties generally tends to increase the T_g, limit the ion mobility and consequently to have a detrimental impact on the resulting ionic conductivity. Such behavior has been reported for different strategies such as the introduction of rigid segments,[27,28] the synthesis of block copolymers by controlled polymerization techniques,[29,30] or the preparation of polymer blends.

Another promising strategy consists in associating a crosslinked or un-crosslinked PIL with a second partner within a (semi-)interpenetrating polymer network ((semi-)IPN) architecture. According to the IUPAC definition, semi-IPNs refers to a material comprising one or more networks and at least one uncrosslinked linear polymer, characterized by an entanglement at the molecular level of these polymer chains within the networks.[31] Although mechanical blending is easier to implement than the elaboration of semi-IPNs, this latter type of architecture provides several advantages over polymer blends. Indeed, semi-IPNs are the only way to combine two polymers of which at least one of the partners is crosslinked. This forced miscibility results in materials that have greater morphological stability over time, better mechanical properties and increased resistance to degradation. Furthermore, (semi-)IPNs can, in some cases, exhibit a true synergy of the properties of each of the partners. In other words, each of the partners acts in a beneficial way on the properties of the other. To date, few works have been reported on this strategy. Vidal et al. first reported in 2006 on combining a sulfonate based PIL network and a polyurethane network leading to an IPN containing 72wt% of PIL network.[32] The formation of the IPN allowed obtaining the film showing according to DMTA the storage modulus as high as 3 MPa, although the conductivity was not reported. In 2015, Shaplov et al. reported the preparation of ionic semi-IPNs by radical copolymerization of an ionic monomer, namely, (*N*-[2-(2-(2-(methacryloyloxy)ethoxy) ethoxy)ethyl]-*N*-methylpyrrolidinium bis(fluorosulfonyl)imide) with poly(ethylene glycol)(di)methacrylates in the presence of the dissolved nitrile butadiene rubber.[33] Such semi-IPNs due to the linear rubber partner involved showed high stretchability and good elasticity (tensile strength 180–430 kPa, elongation 60–180%), but their ionic conductivity was reaching only 1.0×10^{-6} S cm^{-1} at 25 °C. Finally, in 2018, Juger et al. reported the synthesis of an IPN involving the simultaneous formation of the ionic network via copolymerization of ionic methacrylate monomer with poly(ethylene glycol)dimethacrylate and of the reinforcing network via polyaddition of 4,7,10-trioxa-1,13-tridecanediamine with trimethylopropane triglycidyl ether. In that work, the self-standing films have been obtained with storage modulus of 1 MPa and an ionic conductivity as high as 1.5×10^{-5} S cm^{-1} at 25 °C.[34] However, the resulting IPN presented still lower ionic conductivity than the starting PIL and mechanical stretchability was not described.

In all previous works,[33–36] the synthesis of ionic IPNs or semi-IPNs involved the formation of ionic network through copolymerization of ILMs with dimethacrylates, while the reinforcement was provided by incorporated neutral rubbery networks or rubbery linear polymers. Although, the obtained ionic networks demonstrated separately a reasonably low T_g (less than −10 °C), the mobility of polyelectrolyte's chains was limited by the cross-linking nodes and, thus, led to insufficient levels of conductivity. In this work for the first time, we suggested to invert the system by using the highly conductive linear PIL derived from commercial rubber and by reinforcing it by a neutral partner network with synergistic properties (**Figure 1**). As a result, a new family of polymer materials having semi-IPN architecture and presenting both high ionic conductivity and improved mechanical properties suitable for the elaboration of self-standing membranes and thin films has been developed. The ionic conductivity is then provided by the non-crosslinked PIL, bearing ionic liquid-like charge carriers, while the polar PEO network with numerous dangling chains allows decreasing the T_g and increasing the free volume, leading to an enhancement of the ion's mobility. On the other side, while the dimensional stability is insured by the crosslinked nature of the PEO network, the stretchability and mechanical robustness of the resulting materials is enabled by the entanglement of the long PIL chains within the PEO network. Thus, this manuscript describes the synthetic approach toward the formation of the self-standing, soft, flexible, and ion conducting semi-IPN membranes, that were further successfully applied in the liquid-free electrochemical devices by sandwiching them between two formulated poly(3,4-ethylenedioxythiophene):polystyrene sulfonate (PEDOT:PSS) electrodes. Finally, the performances of the resulting truly all-solid-state polymeric actuators and sensors were studied and discussed.

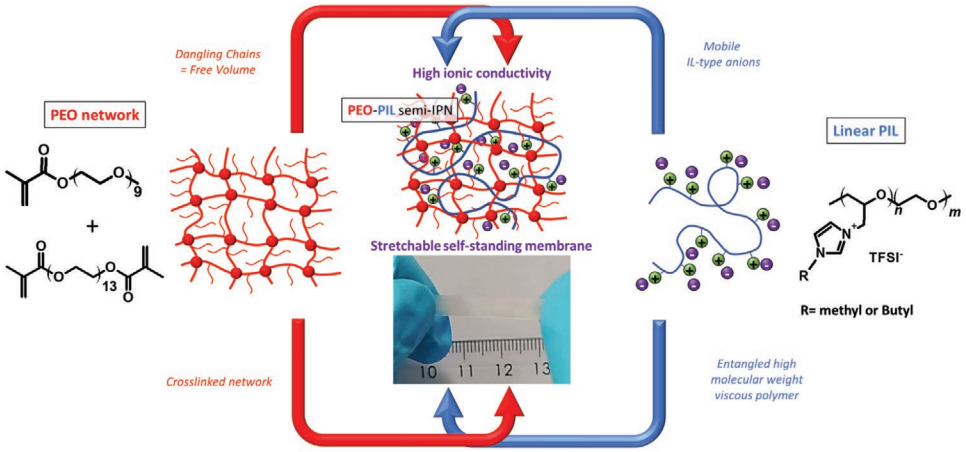

Figure 1. General principle of the polymeric ionic liquid (PIL) materials preparation via a semi-interpenetrating polymer network architecture approach with synergistic properties.

2. Results and Discussions

2.1. Synthesis of Linear PILs

The availability of precursors is a crucial point for the design of the next generation of PILs. In this work two different cationic PILs have been synthesized from commercially accessible poly(epichlorohydrin-*co*-ethylene oxide) (ZEON Hydrin C2000XL) elastomer, which is well known for its high elasticity and good adhesion properties (**Figure 2**a). The first PIL, namely poly(1-methyl-3-(oxiran-2-ylmethyl)-1-imidazole-3-ium-*co*-ethylene oxide) bis(trifluoromethyl-sulfonyl)imide, designated as PIL C1 here, was synthesized according to a protocol published by our group recently.[37] Briefly, the C2000XL precursor first undergone quaternization reaction with *N*-methylimidazole and on the second step the chloride counter-ion was exchanged via metathesis with lithium bis(trifluoromethyl-sulfonyl)imide (LiTFSI).

The synthesis of the second PIL, the poly(1-butyl-3-(oxiran-2-ylmethyl)-1-imidazole-3-ium-*co*-ethylene oxide) bis(trifluoromethylsulfonyl)imide, designated as PIL C4, has been further inspired by literature,[38] including our own previous investigations.[39] Thus, it is known[38,39] that the increase in the length of the cation's substituent can reduce the glass transition temperature (T_g) of the cationic PIL and, as a result, can increase its ionic conductivity. Commonly, such an effect had an extremal character with the maximum of ionic conductivity in PILs having the n-butyl substitutes in imidazolium cation. Thus, the difference between two PILs in this work (Figure 2a) is the length of the alkyl chain on the

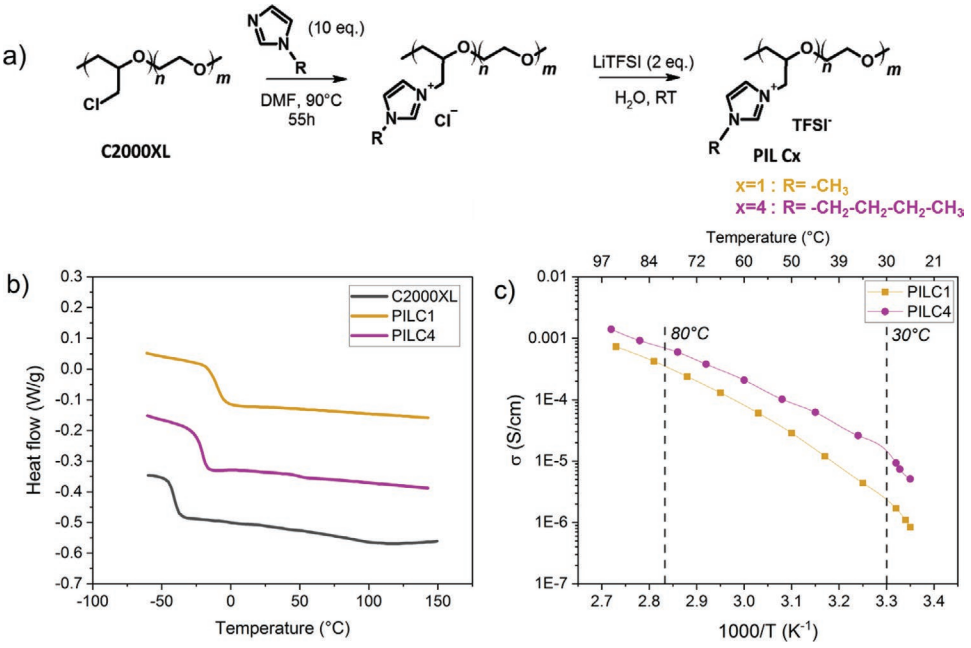

Figure 2. a) Reaction pathway for the synthesis of PIL C1 and PIL C4. b) DSC thermograms of C2000XL precursor, PIL C1 and PIL C4. c) Evolution of the ionic conductivity of PIL C1 and PIL C4 versus the temperature.

imidazolium ring, varying from methyl (PIL C1) to n-butyl (PIL C4). The structure and purity of the prepared cationic PILs bearing mobile $TFSI^-$ counter-ions were characterized by ^1H, ^{19}F NMR, and FT-IR spectra (Figures S1–S3, Supporting Information).

At room temperature, both cationic PILs (Figure 2a) represent transparent cold flowing rubbers and, therefore, do not have sufficient mechanical properties to be processed as membranes. Their thermal transitions have been characterized by dynamic scanning calorimetry (DSC). Figure 2b depicts the thermograms of C2000XL precursor and of two PILs. The C2000XL precursor is amorphous and characterized by a glass transition temperature T_g at –41 °C. The introduction of ionic charge on the backbone of C2000XL induces an increase in T_g up to –16 and –25 °C for PIL C1 and PIL C4, respectively, The T_g of PIL C4 as expected was found to be lower than that of PIL C1 thanks to the longer pendant alkyl chain on the imidazolium ring (methyl vs butyl respectively) due to the increase in free volume.

Ionic conductivity of the synthesized PILs was then measured by electrochemical impedance spectroscopy (EIS). Figure 2c represents the evolution of the ionic conductivity of PIL C*x* as a function of reciprocal temperature (1000/T). At room temperature (25 °C), the ionic conductivity of PIL C1 and PIL C4 was found to be 8.4×10^{-7} and 5.1×10^{-6} S cm^{-1}, respectively. Thus, at 25 °C the ionic conductivity of the PIL C4 is seven times or one order of magnitude higher than that of the PIL C1. With the increase in temperature, the conductivity of both PILs was rising (Figure 2c) and the difference between their values was reducing, reaching 3.8×10^{-4} and 6.9×10^{-4} S cm^{-1} at 80 °C for the PIL C1 and PIL C4, correspondingly. The evolution of the ionic conductivity of a solid electrolyte as a function of temperature can be described according to various laws, the simplest being the Arrhenius relation (Equation (1)):

$$\sigma\ (T) = A \times \exp\left(-\frac{E_a}{RT}\right) \quad (1)$$

where A is a pre-exponential factor independent of temperature, E_a is the thermal activation energy, R is the universal gas constant, T is the absolute temperature (in Kelvin). Another empirical relationship that has been extensively used to describe such evolution is the Vogel–Fulcher–Tammann (VFT) relationship (Equation (2)).[40]

$$\sigma\ (T) = A \times T^{-1/2} \times \exp\left(-\frac{B}{T - T_0}\right) \quad (2)$$

In this equation, A is a term independent of the temperature and contains information about the quantity of charge carriers, B is a fitting parameter related to the pseudo-activation energy of ionic conduction, and T_0 is the reference temperature (Vogel temperature) related to the glass transition temperature of the considered sample. T_0 is generally fixed between 35 and 50 K below the glass transition temperature of the measured sample. In this work, T_0 was set to $T_g - 50$ K.

Experimental data have been plotted according to Arrhenius and Vogel–Fulcher–Tammann (VFT) equations (Figure S4, Supporting Information). Regardless of the PIL's nature, the experimental data fit the VFT model with correlation coefficients (R^2) greater than 0.99 (**Table 1**). Therefore, exactly the VFT model is most suitable for the description of their ionic behavior, and within these PILs, the motion of the charge carriers is correlated with the segmental movement of the polymer chains as it has already been extensively described elsewhere.[40] When the VFT parameters are analyzed in detail (Table 1), it can be noticed that the value of the A parameter increases from 94 to 137 S cm^{-1} K$^{-1/2}$ for the PIL C1 and the PIL C4, respectively. Since both PILs have almost the same amount of charge carriers (i.e., 2.24 and 2.06 mmol g^{-1} of polymer, respectively), such variation of the parameter A cannot be only explained by this small difference. Furthermore, the value of the parameter A of the PIL C4 is higher than that of PIL C1 even though it contains fewer ionic charge carriers per gram of polymer. Therefore, a distinction should be made between the whole amount of charge carriers and the amount of charge carriers available and participating in the ionic conduction phenomenon. Indeed, beyond a certain ionic species concentration threshold, it is likely that the counter-ions start to form ion pairs and aggregations that do not participate on the overall ionic conductivity of the PIL.[20] The presence of longer alkyl chain on PIL C4 imidazolium likely hinders interactions between charge carriers, consequently reducing the formation of ion pairs and aggregations. This will lead to a higher available amount of charge carriers in the case of PIL C4 in comparison with PIL C1. The higher ionic conductivity of PIL C4 at room temperature is also explained by its lower pseudo-activation energy (i.e., parameter B). Its lower value for PIL C4 can be interpreted by lower glass transition temperature allowing polymer chains to exhibit greater flexibility and mobility and, thus, a better ionic motion since both are correlated.

Table 1. Fitted parameters of the Vogel–Fulcher–Tammann (VFT) equation for PIL C1 and PIL C4.

	A [S cm^{-1} K$^{-1/2}$][a)]	B [K][a)]	$R^{2b)}$
PIL C1	94	1443	0.9982
PIL C4	137	1376	0.9968

[a)]The values of parameters A (term independent of the temperature, that contains information about the quantity of charge carriers) and B (fitting parameter related to the pseudo-activation energy of ionic conduction) for Equation (2), obtained from the best fittings of the experimental curves (Figure 2c); [b)] The R-squared or the coefficient of determination for the obtained parameters A and B of the Equation (2).

In summary, the two studied cationic PILs are amorphous, possess low T_g and exhibit sufficiently high ionic conductivity of ≈10^{-6} S cm^{-1} at 25 °C, which is reaching two orders of magnitude higher values at 80 °C (≈10^{-4} S cm^{-1}). However, due to low glass transition temperatures both PILs represented cold flowing rubbers and thus showed no dimensional stabilities. In order to obtain self-standing solid polyelectrolyte films, the combination of PIL C1 or PIL C4 with a second polymeric network partner was suggested.

2.2. Synthesis of Semi-IPNs

The combination of PIL C*x* (x = 1 or 4) with a second partner was performed via a semi-IPN architecture in which the linear PIL acts as the ionic partner bringing the mobile charge carriers

and ionic conductivity, respectively. As the latter is intimately correlated with the polymer backbone motion, the preservation of such thermodynamic motion is essential for maintenance of high overall system conductivity and thus, for the first time we proposed to keep the linear structure of PIL during the synthesis of a semi-IPN architecture. The choice of the second partner polymer network focused on a dangling-chains PEO network already described in the literature and used in the development of electroactive devices.[26] Verge et al. showed that a PEO network composed of 75 wt% of poly(ethylene glycol) methacrylate (PEGM) and 25 wt% of poly(ethylene glycol) dimethacrylate (PEGDM) presents an ideal compromise between the contribution of mechanical and ion transport properties within the same material.[41] This kind of network offers several advantages: on one hand the PEGDM, as a crosslinker, provides the required mechanical properties to obtain a dimensionally stable material, while the presence of PEGM promotes ionic mobility due to its polarity as well as the free volume provided by its dangling chains.

In this paper, PEO/PIL semi-IPNs were synthesized by an in situ process where both components have been solubilized in the same solvent and the crosslinking process of the PEO network takes place in the presence of already synthesized PIL (**Figure 3**a). For each semi-IPN composition, the PEO network was composed of 75 wt% of PEGM and 25 wt% of PEGDM. PIL C*x*, PEGM, PEGDM, and DCPD as free radical initiator were solubilized in cyclohexanone and the PEO network was then prepared at 50 °C by free radical copolymerization of PEGM and PEGDM. Two families of semi-IPNs were synthesized: PEO/PIL C1 and PEO/PIL C4. For each family of semi-IPNs, the weight ratio of PEO network has been varied from 40 to 90 wt%. Although theoretically only the physical entanglement between a linear PIL and PEGM/PEGDM network should be present in the obtained semi-IPNs, the minimal chemical bonding between the ethylene oxide fragments of both partners could also happened due to the utilization of peroxide DCPD initiator.[42]

In order to follow the formation of the PEO networks, a rheological study in the dynamic mode of the crosslinking kinetics was therefore carried out. The evolution of the storage modulus *G′* of the reactive mixture was followed regarding time and temperature for PEO/PIL C1 and PEO/PIL C4 semi-IPNs in Figures 3b and 3c, respectively. For all semi-IPNs studied the evolution of the storage modulus follows the same behavior. In the first part of the synthesis (3 h at 50 °C), the modulus increases gradually and then reaches a plateau value comprised between 0.12 and 0.21 MPa regarding the PEO content. The higher was the content of PEO in the semi-IPN composition, the faster this plateau was reached due to the increase in monomer concentration. Although the modulus reaches a plateau value at 50 °C, it should be noted that during the increase of the temperature from 50 to 80 °C, the storage modulus systematically increased and reached values between 0.32 and 0.87 MPa. Such continuous increase in modulus proves that not all methacrylate functions have reacted at 50 °C, underlining the necessity in the post-curing step. The invariability of the storage modulus at 80 °C further suggests that the majority of methacrylate functions has reacted. When the content of PEO within the semi-IPN is reduced to only 40 wt%, the storage modulus at the end of the polymerization was barely reaching 100 Pa and the resulting materials demonstrated a viscous-like behavior. This observation could be explained by too low amount of

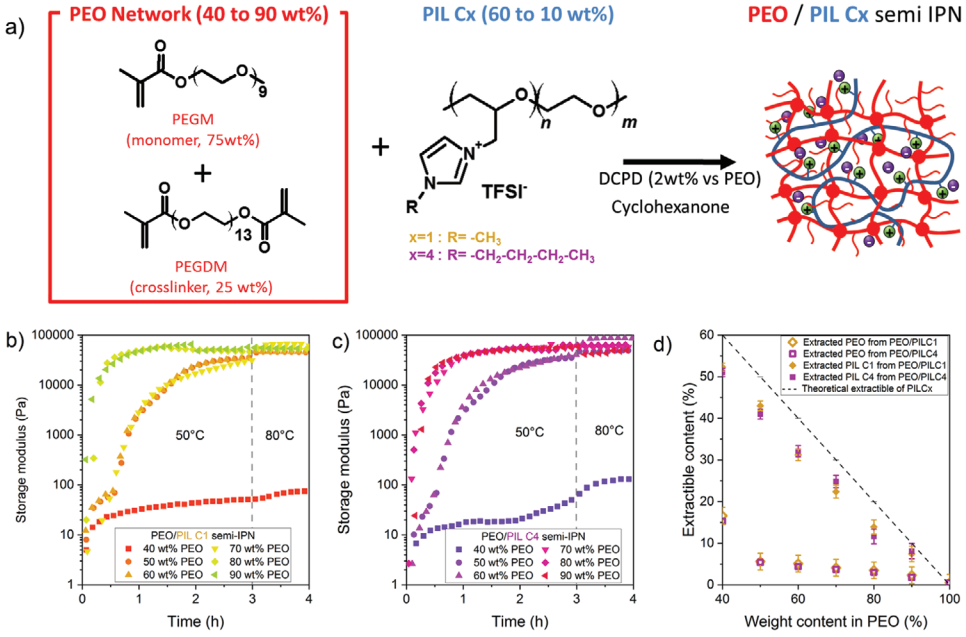

Figure 3. a) Schematic presentation of the semi-IPN synthesis based on linear PIL and a PEO network. Storage modulus (*G′*) versus temperature and time dependence during the synthesis of b) PEO/PIL C1 and c) PEO/PIL C4 semi-IPNs. d) Extractible content of PEO network and of linear PIL C*x* from PEO/PIL C*x* semi-IPNs measured by solid/liquid Soxhlet extraction in ethanol (extraction of uncrosslinked PEO precursors only) and deducted from the difference between solid/liquid Soxhlet extraction in ethanol and in acetonitrile (extraction of both linear PIL and uncrosslinked PEO precursors), respectively.

the PEO precursors to form the reinforcing network, instead leading to the formation of PEO microgels without network percolation and preventing the dimensional stability of the films. To avoid this situation happened, the minimum content of PEO in the semi-IPNs was set at 50 wt%.

While the rheological characterizations have allowed the evidence of the network formation, the completion of crosslinking reaction was not fully proved. The latter has been additionally verified by the measurement of extractible contents by means of solid/liquid extraction using a Soxhlet extractor. As these materials are semi-IPNs, it was necessary to find such a solvent that will allow to differentiate between the extraction of unreacted PEO precursors and of the linear PIL C*x*. To do so, the removal of uncrosslinked PEO components was carried out in ethanol, which is a good solvent for PEO network precursors and does not dissolve any of PIL C*x* even at high temperatures. Figure 3d represents the extractible content of semi-IPNs as a function of PEO network composition using ethanol as a solvent. For a PEO content of 40 wt% and regardless the type of PIL C*x*, the extractible content was around 16%. This relatively high value is explained by the fact that, at such low content of loaded PEO precursors, the formation of the continuous reinforcing PEO network does not occur as highlighted in the rheological measurements section. In contrast, the PEO precursors are capable only of microgels generation, that are dispersed within the membrane and possess a significant quantity of uncrosslinked methacrylic monomers and oligomers. On the other hand, when the amount of loaded PEO precursors exceeded 50 wt%, the values of extractible content for all generated films were found to be below 5%, indicating that in these conditions the applied thermal treatment was sufficient to satisfactorily crosslink the methacrylic functions and to successfully generate the continuous PEO network within respective semi-IPN.

On the next step, the extraction has been performed using acetonitrile as a solvent capable to dissolve both linear PIL C*x* and unreacted PEO network precursors. At this, the extractible content of linear PIL C*x* can be calculated from the difference between the extractible contents in acetonitrile and those in ethanol (Figure 3d). In all studied semi-IPNs, the extractible content of PIL C*x* was very close to the amount of PIL C*x* loaded during the synthesis of the semi-IPN membranes, indicating that it is possible to extract almost the entire amount of PIL partner. These results confirm that PIL C*x* polymer chains are merely physically entangled within the PEO network and thus prove the formation of a semi-IPN architecture. A slight difference systematically observed between the experimental extractible content and the loaded amounts of linear PILs can be potentially attributed to the difficulty of high molecular weight polymers extraction and in part to the possible limited grafting side-reactions.

2.3. Thermomechanical Characterizations of the Semi-IPNs

To provide a convenient combination of ionic conductivity and mechanical properties in the semi-IPN, a co-continuous morphology is desirable. Thus, the quality of interpenetration of networked PEO and linear PIL C*x* has been studied by DSC and DMA.

At first step, all semi-IPNs have been characterized by DSC. The complete thermograms of the semi-IPNs (Figure S5, Supporting Information) show that all these materials are amorphous and exhibit one glass transition temperature (T_g). The measured onset T_g versus PEO network content dependences are reported in **Figure 4**a. The determined onset T_g values for semi-IPNs varied from −33 and −40 °C for 40 wt% of PEO content to −55 and −56 °C for 90 wt% for PIL C1 or PIL C4, respectively. The higher was the content of PEO network within the semi-IPN, the lower was the observed T_g, shifting to that of the PEO network alone (−57 °C). Generally, the study of the DSC thermograms also allows to deduce the information about the level of interpenetration between the partners of a polymer blend. Indeed, two polymers with large difference in T_g can be considered as perfectly interpenetrated if only one glass transition is observed for the material. In this study, the ΔT_g ($|T_{g(\text{PIL C}x)} - T_{g\text{PEO}}|$) is about 35 °C, which is sufficiently high value according to literature.[43] Regardless the PIL C*x* used in the semi-IPN preparation, only one T_g was observed, that in its turn suggests good level of interpenetration between the linear PIL C*x* and PEO network. At the same time, the semi-IPNs containing 40 and 50 wt% of PEO network showed more pronounced and clearer step-like transition, while samples with 60 and 70 wt% of PEO demonstrated more blurry transitions (Figure S5, Supporting Information). This allows to state that the level of interpenetration and compatibility is higher in semi-IPNs with 40 and 50 wt% of PEO network.

To go further in the data analysis, mathematical models were applied to predict the T_g of polymer blends as a function of their composition and taking into consideration different possible interactions between the partners. Three different models, namely Fox, Gordon–Taylor and Kwei, have been used to fit the evolution of the T_g versus the PEO network content (Figure S6, Supporting Information). As it can be clearly observed from Figure 4a and Figure S6, Supporting Information, only the Kwei's equation, which predicts the strongest interactions between the two components, demonstrates the best fitting with experimental results having a correlation coefficient above 0.99. It proves the strong interactions existing between the ionic moieties of linear PIL with ethylene oxide repeat units in both the backbones of PIL and PEO network as well as with PEO dangling chains via hydrogen bonding as reported elsewhere.[44] Such strong interactions between the polymer chains clearly explain why only the one T_g is observed in DSC for all of the semi-IPNs compositions.

The viscoelastic behavior of semi-IPNs materials has been further characterized by dynamic mechanical analysis (DMA). The temperature behavior of the loss factor (tan δ) for neat PEO network and for both PEO/PIL C1 and PEO/PIL C4 semi-IPNs is provided in Figure 4b,c, while the evolution of the storage modulus (E') as a function of temperature is given in Figure S7, Supporting Information. Unfortunately, PIL C*x* linear polymers could not be studied by the DMA method for comparison as at room temperature they both represent cold flowing rubbers and are not capable to form the self-standing films. The neat PEO network showed a single α relaxation with a maximum of tan δ at −38 °C (Figure 4b). Similarly, all semi-IPNs irrespectively to the PEO content and the nature of PIL C*x* demonstrated only one T_g (T_α more precisely) on loss factor curves (Figure 4b,c).

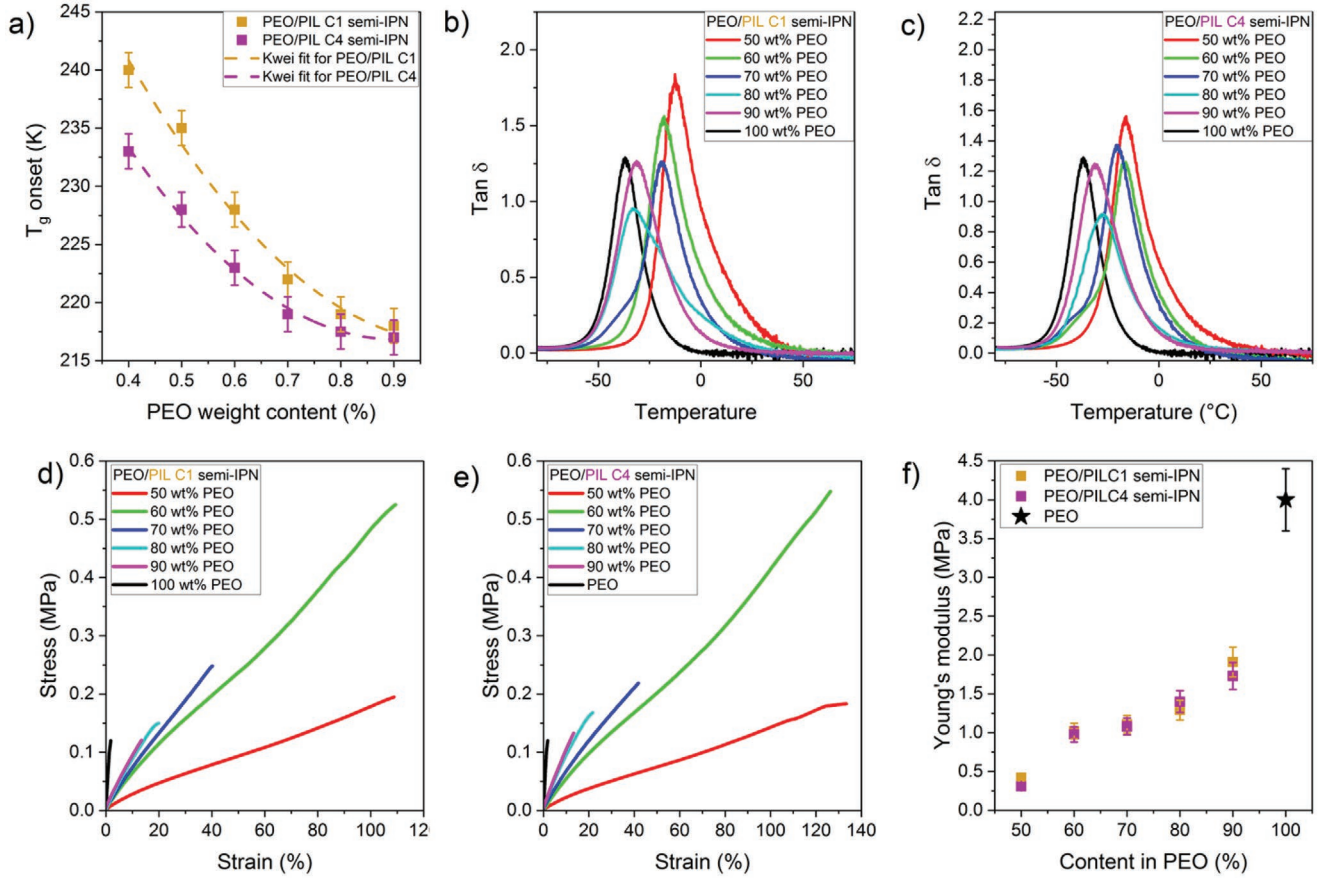

Figure 4. a) Evolution of the onset T_g values of PEO/PIL C1 and PEO/PIL C4 semi-IPNs as a function of their composition and a mathematical fit of the T_g experimental data using Kwei model. Temperature evolution of the loss factor tan δ for b) PEO/PIL C1 and c) PEO/PIL C4 semi-IPNs as a function of their composition. Stress–strain curves of d) PEO/PIL C1 and e) PEO/PIL C4 semi-IPNs as a function of their composition at 25 °C. f) Evolution of the Young modulus of PEO/PIL C*x* semi-IPNs as a function of their composition.

The shift in T_g from –13 to –35 °C was observed for semi-IPNs with the increase in PEO network content from 50 to 90 wt%. At this, the T_g of semi-IPNs with PEO content as high as 90 wt% was found to be close to the α relaxation of the neat PEO network. It is necessary to mention, that for the several semi-IPNs, namely for 70/30 PEO/PIL C1, 60/40 PEO/PIL C4, and 70/30 PEO/PIL C4 a slight shoulder on the low temperatures side was visible (Figure 4b,c). Most probably this can be explained by the presence of some phases richer in PEO partner rather than by the segregation of the two components. The observation of a single α relaxation indicates that, at the DMA scale (50 nm),[45] the networked PEO and linear PIL C*x* are well interpenetrated and represent homogeneous materials, that is in a full agreement with the DSC analysis for which only one T_g was noted for all semi-IPNs.

The stress-strain curves at 25 °C are shown in Figure 4d,e for PEO/PIL C1 and PEO/PIL C4 semi-IPNs, respectively. The neat PEO network exhibits a stress 0.15 MPa and an elongation at break equal to 4% only. Such rigid or brittle-like behavior can be explained by the high degree of crosslinking nodes in this material. For semi-IPNs both tensile strength and elongation at break were found to be independent on the nature of the PIL C*x* and to be controlled by the content of PEO network. When PEO content decreased, the elongation at break was increasing significantly from 13% to more than 100% from 90/10 PEO/PIL C*x* to 60/40 PEO/PIL C*x* semi-IPN, respectively. This can be explained by the decrease of the weight fraction of highly crosslinked PEO network and by the increase, at the same time, of the weight fraction of entangled linear PIL C*x*. The same was observed for the stress at break which was increasing from 0.12 MPa for 90/10 PEO/PIL C*x* to more than 0.5 MPa for 60/40 PEO/PIL C*x* membranes. The situation changed for the semi-IPN with 50 wt% of PEO content, for which the tensile strength suddenly drops to 0.2 MPa indicating a poor continuity of the PEO phase for this composition.

Figure 4f summarizes the evolution of the Young modulus versus the variation in PEO content of the semi-IPNs. The neat PEO network demonstrated Young modulus of 4 MPa. When the weight content of PEO decreased in the composition of the semi-IPNs, the Young modulus was decreasing as well, reflecting the softening of the resultant materials. In such a way, the Young modulus was continuously decreasing from 1.3 to 1.0 MPa during the transfer from 80/20 to 60/40 PEO/PIL C*x* semi-IPNs. The exception was again found for the 50/50 PEO/PIL C*x* membranes, for whom the Young modulus was suddenly dropping to 0.3 MPa (Figure 4f). This observation is in agreement with the hypothesis of poor continuity of the partners in 50/50 PEO/PIL C*x* materials mentioned above and

suggests that the co-continuous morphology was obtained for the semi-IPNs with PEO content strictly higher than 50 wt%.

Finally, whatever the PIL C*x* used within the semi-IPN, an optimum of the mechanical properties was obtained for a composition of 60/40 PEO/PIL C*x*. Thus, for 60/40 PEO/PIL C1 and 60/40 PEO/PIL C4 the tensile stress was found to be 0.52 and 0.55 MPa, while the elongation at break varied between 109% and 126%, respectively. Such composition was providing the highest tensile properties probably due to the optimum combination of the dimensional stability coming from the networked PEO partner and elasticity derived from the entanglement of the linear PIL C*x*.

2.4. Ionic Conductivity of the Semi-IPNs

All ionic conductivities of semi-IPNs were measured in anhydrous conditions under inert atmosphere (argon). The evolution of the ionic conductivity at 30 °C as a function of the PEO network content is given for the two semi-IPNs in **Figure 5**a. Independently on the nature of the PIL C*x*, the evolution of the ionic conductivity as a function of the PEO network content seems to exhibit similar behavior. First, when the PEO content increased from 0 to 60 wt%, the ionic conductivity of the semi-IPNs was increasing from 5.1×10^{-6} to 8.7×10^{-5} S cm^{-1} (30 °C) in the case of the semi-IPN PEO/PIL C4, for example. Then the dependence was passing through the maximum at 3.8×10^{-5} and 8.7×10^{-5} S cm^{-1} (30 °C) for 60/40 PEO/PIL C1 and 60/40 PEO/PIL C4, respectively. Thus, the highest ionic conductivity was observed for each semi-IPN family at a composition containing 60 wt% of PEO network (Figure 5a). It should be underlined that in these cases, the ionic conductivity is more than an order of magnitude higher than those of corresponding PIL C*x* alone. This observation therefore highlights the beneficial role of the PEO network presence on the ionic conductivity of the studied materials. Several phenomena can be involved: i) A better dissociation of the ion pairs with the increase of the PEO content, which could lead to an increase in the quantity of mobile ions truly available for the ionic transport process and/or ii) an increase in the free volume within the semi-IPNs by increasing the content of dangling chains provided by the PEO partner, which decreases the T_g and thus would increase the polyelectrolyte backbone motion and the mobility of the counter ions. Lastly, when the PEO content in semi-IPN was increased above 60 wt%, the ionic conductivity of the membranes started to decrease, probably due to the dilution effect that reduces the charge carrier concentration.

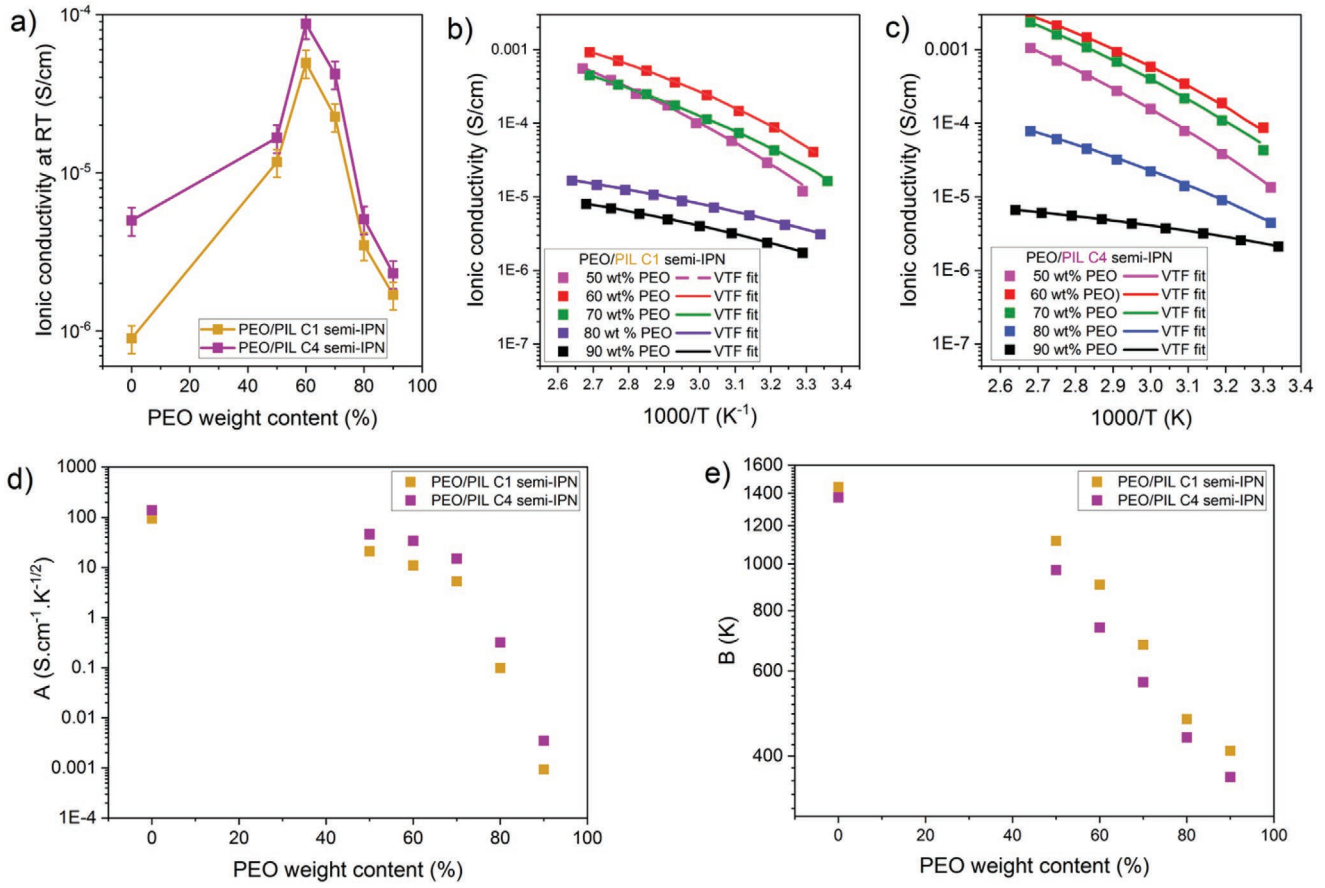

Figure 5. a) Evolution of the PEO/PIL C*x* semi-IPNs ionic conductivity at 30 °C as a function of their composition. Temperature evolution of the b) PEO/PILC1 and c) PEO/PILC4 semi-IPNs ionic conductivity as a function of their composition of and the corresponding VTF fit curves. Evolution of the VTF d) A and e) B parameters as a function of PEO/PIL C*x* semi-IPNs composition.

The study of the ionic conductivity evolution as a function of temperature was performed for each semi-IPN composition (Figure 5b,c). For all semi-IPNs the ionic conductivity was rising with the increase in temperature. For example, for 60/40 PEO/PIL C1 and 60/40 PEO/PIL C4 semi-IPNs, the ionic conductivity was increasing from 3.8×10^{-5} to 9.0×10^{-4} and from 8.7×10^{-5} to 3.1×10^{-3} S cm^{-1}, when the temperature was rising from 30 to 100 °C, which is approximatively a 30-fold increase in the ionic conductivity. Whatever was the nature of PIL C*x*, the increase in PEO content in the semi-IPN was leading to less dependence of the ionic conductivity on temperature. For example, for the 90/10 PEO/PIL C*x* semi-IPNs, the ionic conductivity was only increasing by a factor of 4 with the rise in the temperature from 30 to 100 °C (Figure 5b,c). The achieved experimental values of ionic conductivity were fitted with the VTF model (Figure 5d). For all participated semi-IPNs the correlation coefficient was equal to 0.996, on average. Thus, it can be concluded that the materials under study similarly to linear PIL C*x* follow the VTF behavior which states that, the ionic conductivity is not only governed by the movement of the mobile charge carriers, but is also affected by the segmental motion of polymer chain. The evolution of the VTF parameters (i.e., *A* (S cm^{-1} K$^{-1/2}$) and *B* (K)) is reported as function of the PEO content in Figure 5d,e. Both parameters *A* and *B* were rapidly increasing with the decrease in PEO content from 90 to 70 wt% and were reaching the plateau at ≈60 wt% of PEO content. Such a behavior of parameters *A* and *B* can additionally explain the maximum of ionic conductivity observed for the 60/40 PEO/PIL C*x* semi-IPNs by a trade-off between the reduction in the quantity of the mobile charge carriers and the increase in their mobility.

2.5. Application in Flexible All Solid-State Electrochemical Devices

Being inspired by the creation of a new family of polymer materials, namely the ionic semi-IPNs, that showed simultaneously the excellent tensile properties and high ionic conductivity in anhydrous conditions, it was further decided to study their potential as separator membranes in flexible all-solid-state electrochemical devices such as electrochemical ionic actuators and piezoionic sensors. The 60/40 PEO/PIL C*x* semi-IPNs having the highest conductivity and optimum tensile properties were used for the fabrication of self-standing trilayer devices in combination with two electronically conducting polymer electrodes (**Figure 6**). Such device structure corresponds to the simplest configuration of an electrochemical cell, that is, two electroactive electrodes are separated by an electrolytic or ion conducting medium necessary for oxidation-reduction processes. At this, there is no need in any additional stiff current collector or encapsulating layers that would otherwise participate to the mechanical properties of the whole device. The poly(3,4-ethylenedioxythiophene):(polystyrene sulfonate) (PEDOT:PSS) has been chosen as an electronic conducting polymer (ECP) for the fabrication of the soft and flexible electrodes. This ECP is commercially available in an aqueous dispersion form and has the advantage of being easily processed through various well reported methods, such as drop casting, spray coating, spin-coating, and ink-printing techniques[46,47] with various formulations and treatment to improve their properties.[48] Three types of PEDOT:PSS electrodes have been used for the preparation of the trilayer devices: i) pristine PEDOT:PSS coating, ii) PEDOT:PSS formulated with

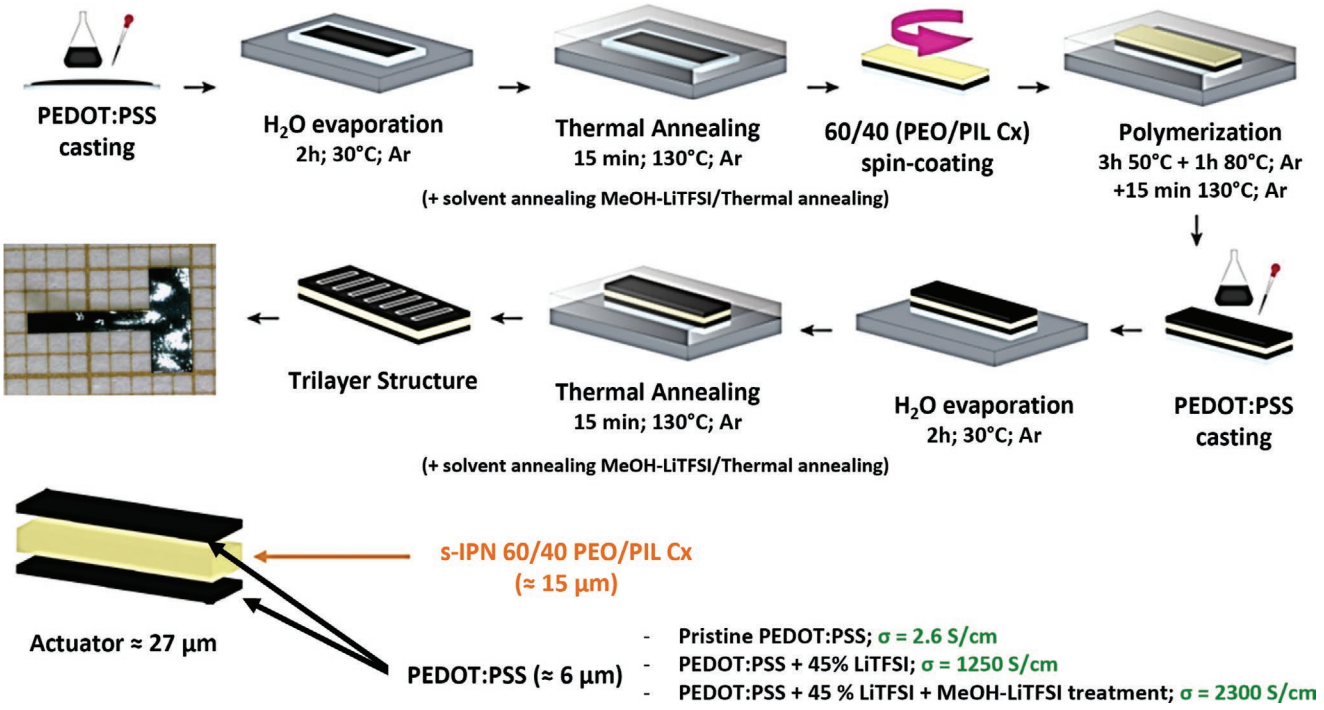

Figure 6. Schematic representation of the elaboration of pseudo-supercapacitors based on modified PEDOT:PSS electrodes by a stacking/polymerizing process.

45.5 wt% of LiTFSI as an electronic conductivity enhancer additive, and iii) PEDOT:PSS formulated with 45.5% of LiTFSI and post-washed with LiTFSI/MeOH, according to previously reported method.[49] The resulting three electrodes present a thickness of ≈6 µm and electronic conductivities measured by four-probe method equal to 2.6, 1250, and 2300 S cm^{-1} (25 °C), respectively. Eventually, the trilayer devices were fabricated by a stacking/polymerization method as shown in Figure 6, according to a previously describe procedure,[50] that concludes in following steps: i) casting of the PEDOT:PSS dispersion onto a silicon substrate to form the bottom electrode; ii) spin-coating of the PEO/PIL C*x* semi-IPN precursors onto the surface of the bottom electrode with subsequent radical polymerization, leading to the formation of a 15 µm-thick central membrane; iii) casting of the PEDOT:PSS dispersion again on top of the resulting membrane to form the top electrode. At the end of the elaboration process, the trilayer devices with a total thickness of around 27 µm were obtained. They were cut into T shape (Figure 6) architecture comprising the free bending beam (6 mm × 1 mm) and a base for clamping between the electrical contacts (5 mm × 2 mm).

2.5.1. All-Solid-State Actuators

As an ionic actuator, the trilayer device can convert the opposite faradic processes occurring at the electrodes under low voltage (<2 V), that is, oxidation of one electrode and concomitantly to the reduction of the other one, into opposite volume variations of the electrodes (expansion/contraction) and then into large bending deformation. Such electromechanical response is occurring due to the insertion/expulsion of ions exchanged between the electrodes and the middle electrolyte membrane in order to insure the overall electroneutrality. The beam is then stimulated by applying a +2 V potential step for 60 s and measuring the corresponding displacement with a Laser displacement sensor (real-time videos available as Supporting Information). Since the amplitude of the electromechanical response can be strongly influenced by the geometry of the beam, the strain difference of the electrodes is calculated.[51] **Figure 7**a depicts the evolution of the strain difference of trilayer devices as a function of the time for the PEO/PIL C4 semi-IPN combined with each of the three PEDOT:PSS electrodes. All the three assembled trilayer devices were capable to demonstrate perfect bending deformation upon electrical stimulation, thus confirming the efficiency of the semi-IPN as all-solid-state ion conducting electrolyte. The amplitude and the rate of the electromechanical response was however strongly influenced by the type of electrodes used. After only 5 s, the deformation was reaching around 0.08% for the poorly conducting (2.6 S cm^{-1} at 25 °C) neat PEDOT:PSS electrodes. However, it increased significantly up to the 0.49 and 0.88% for the PEDOT:PSS electrodes formulated by the two other methods and having crucially higher electronic conductivities (1250 and 2300 S cm^{-1} at 25 °C). After 60 s, the strain difference was reaching the values of 0.28%, 0.8%, and 1.03%, respectively. While the difference in response rate can be directly associated with the increase in electronic conductivity of the electrodes, the amplitude of the maximum of deformation is simultaneously strongly dependent on the electrochemical charge density of the electrodes.[52] The volumetric charge density of the electrodes has been measured separately for each trilayer device by the integration of the cyclic voltammetry plots performed in a two-electrode configuration at 20 mV s^{-1} between +2 and −2 V. The volumetric charge density was reaching 2.5 × 10^7, 8.65 × 10^7, and 1.25 × 10^8 C m^{-3} with the increase in electrodes conductivity from 2.6 to 2300 S cm^{-1} correspondingly (Figure 7b). The inset on Figure 7b visually demonstrates that the dependence of strain difference as a function of the volumetric charge density of the electrodes possesses linear behavior, thus proving the strong influence of the electrodes properties on the electromechanical response of the actuating devices. The influence of the PEO/PIL C*x* semi-IPN nature was investigated by measuring the strain difference as a function of time for 60/40 PEO/PIL C1 and 60/40 PEO/PIL C4 semi-IPNs coupled with the most conducting PEDOT:PSS electrodes (2300 S cm^{-1} at 25 °C). Figure 7c shows that the both curves present identical shape with a fast increase in deformation within 5–6 s and afterward reaching the plateau or the so-called saturation regime. The device elaborated with 60/40 PEO/PIL C4 membrane appears to be faster (initial strain difference rate 0.15% s^{-1}) than the one assembled with 60/40 PEO/

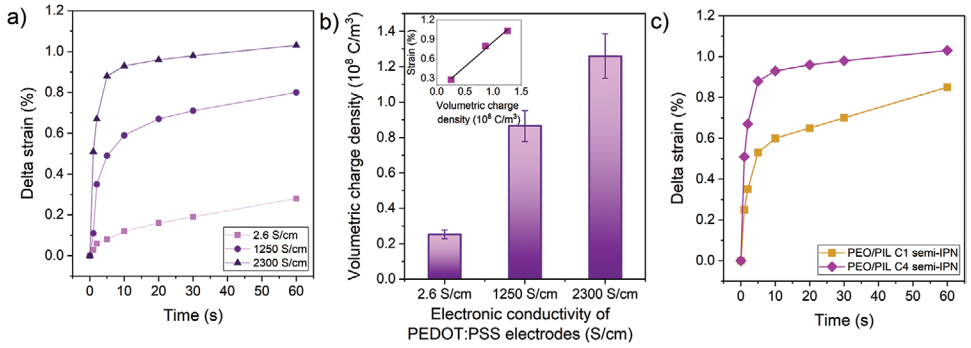

Figure 7. a) Time evolution of the strain difference with a step 2 V voltage sweep during 60 s for trilayer PEDOT:PSS‖60/40 PEO/PIL C4‖PEDOT:PSS actuators with three different PEDOT:PSS electrodes. b) Volumetric charge density of the PEDOT:PSS electrodes measured by cyclic voltammetry (20 mV s^{-1}, [−2 V; +2 V]) in the trilayer actuators with the linear dependency of the strain difference versus the volumetric charge density of the electrodes (inset). c) Time evolution of the strain difference with a step 2 V voltage sweep during 60 s for trilayer PEDOT:PSS‖60/40 PEO/PIL C1‖PEDOT:PSS and PEDOT:PSS‖60/40 PEO/PIL C4‖PEDOT:PSS actuators combined with highly conducting PEDOT:PSS electrodes (2300 S cm^{-1}).

PILC1 (0.10% s^{-1}), that can be explained by faster ionic motions in 60/40 PEO/PIL C4 film and respectively by its higher ionic conductivity. The lower deformation obtained after 60 s for the actuator elaborated with 60/40 PEO/PIL C1 membrane can be assign to the fact that the saturation plateau has not been reached yet after 60 s due to the slower electromechanical processes associated with this membrane (Figure 7c; Figure S8, Supporting Information). Nevertheless, the obtained results highlight that the PEO/PIL C*x* semi-IPNs are unique and productive electrolytes allowing the construction of efficient, flexible, and truly all-solid-state electrochemical ionic actuators. Moreover, the effectiveness and the performance of the solid-state devices based on the developed semi-IPNs were equal to or even exceeding those of the "wet" systems having the central membrane swollen with liquid electrolytes or ionic liquids (see for example,[50] where the actuator showed a strain difference rate of 0.16% s^{-1} at the similar potential).

2.5.2. All-Solid-State Sensors

The all-solid-state trilayer devices were further investigated as soft mechanical sensors (**Figure 8**). As a piezoionic sensor,[53] the trilayer device converts a bending deformation into a flux of ions due to a pressure gradient mechanically generated from the compressed side of the film to the expanded one. Such unbalanced distribution of ions results in a variation of the open-circuit voltage that can be then measured and used to detect and quantify the amplitude of the deformation.[53] Step deformation was first applied (Figure 8a) to the trilayer sensors with highly conducting PEDOT:PSS electrodes (2300 S cm^{-1}) and the resulting open-circuit voltage (OCV) variation between the two electrodes of the device was recorded over time. Interestingly, when a step displacement is applied, a step variation of the OCV with limited voltage relaxation is observed for both sensors: based on 60/40 PEO/PIL C1 and 60/40 PEO/PIL C4 (Figure S9, Supporting Information). The Figure 8b plots the OCV variation as a function of the applied strain difference. A relatively linear evolution is observed confirming that the assembled devices can be effectively used not only to detect pressure, but also to quantify the mechanical deformation. The sensitivity slope detected for both PEDOT:PSS/60/40 PEO/PIL C*x*/PEDOT:PSS sensors was as high as 0.64 mV/%. It should be mentioned that such elevated level of sensitivity was obtained for truly all-solid-state devices, while similar or closed values (0.74 mV/%) were achieved only for "wet" polymer systems swollen with ionic liquids. These results undoubtedly demonstrated the future perspectives of the solid state piezoionic sensors and the importance to design novel highly conducting PILs and networked materials on their bases.

3. Conclusions

In summary, the work carried out and reported in this paper has elaborated the new method for the development of novel all-solid-state polyelectrolyte membranes with semi-IPN architecture. These newly synthesized semi-IPNs differ from the known ones by reverse combination of partners, namely by blending a linear ion conducting polymeric ionic liquid (PIL) with reinforcing PEO network derived from copolymerization of poly(ethylene glycol) methacrylate methyl ether and poly(ethylene glycol) dimethacrylate. The semi-IPNs formation kinetics was investigated by rheological measurements, while their mechanical and thermal properties were studied by rheology, dynamic scanning calorimetry (DSC), dynamic mechanical analysis (DMA), and stress–strain measurements. The ionic conductivity was assessed by electrochemical impedance spectroscopy (EIS). It was revealed that for the ratio of 60 wt% of PEO network and 40 wt% of linear PIL C*x*, a true synergy of ionic conductivity and mechanical properties has been obtained. It was demonstrated that the association of a linear PIL with a polar PEO network owning dangling chains facilitates the ions movement within the material and significantly enhances the ionic conductivity of semi-IPNs in comparison with neat linear PIL C*x*. The highest ionic conductivity of 8.7×10^{-5} S cm^{-1} at 30 °C was gained for 60/40 semi-IPNs based on PIL C4, which, to the best of our knowledge, is among the highest ever reported in literature for PILs in anhydrous conditions (see Table S1, Supporting Information). At the same time, these 60/40 PEO/PIL semi-IPNs have shown improved mechanical properties compared to those of the partners alone. This was explained by two factors: a) on one hand, the crosslinking of PEO network within the semi-IPN provided a

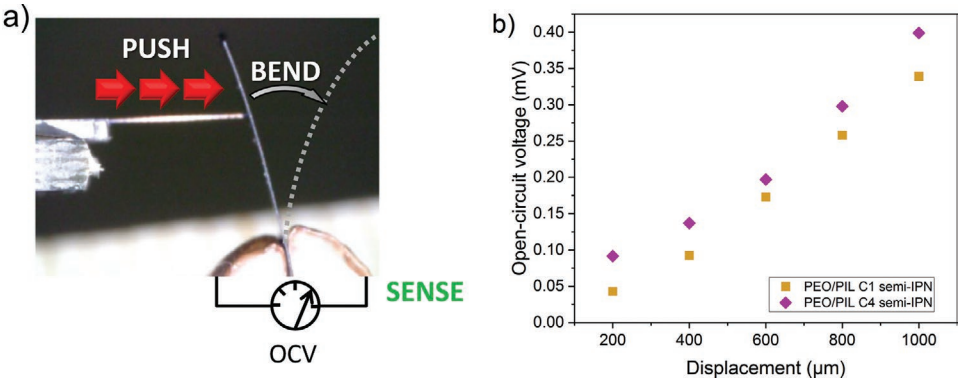

Figure 8. a) Picture showing the principle of the measurement in sensing mode for the PEDOT:PSS||PEO/PIL C*x*||PEDOT:PSS trilayer films. b) Variation of the open-circuit voltage (OCV) during bending deformation as a function of the applied strain difference for the trilayers composed of PEO/PIL C1 or PEO/PIL C4 and highly conducting PEDOT:PSS electrodes (2300 S cm^{-1}).

dimensional stability to the resulting material, allowing self-standing membranes ($E \approx 1$ MPa); b) on the other hand, due to entanglement of the linear PIL C*x*, the semi-IPN membranes could undergo large deformations, thus leading to significant strain at break (>100%). The resultant properties of the 60/40 semi-IPN membranes proved a truly synergistic behavior where each partner acted in a beneficial way, that led to the superior properties in comparison with each partner taken solely.

As a proof-of-concept, the application of the obtained semi-IPNs for the assembly of flexible all-solid-state electrochemical devices such as ionic actuators and piezoionic sensors was successfully demonstrated. For this purpose, the 60/40 PEO/PIL C*x* semi-IPNs having the highest conductivity and enhanced tensile properties were combined with two electronically conducting poly(3,4-ethylenedioxythiophene):polystyrene sulfonate (PEDOT:PSS)-based polymer electrodes, thus forming a trilayer structure. The assembled ionic actuators showed the deformation of 0.88% after only 5 s of current application, while after 60 s the strain difference was reaching the value of 1.03%. The piezoionic sensors based on PEO/PIL C*x* semi-IPNs demonstrated the sensitivity slope as high as 0.64 mV/%.

To conclude, the most striking advantages of the ionic semi-IPNs with new architecture are 1) the formation of self-standing soft elastic films with excellent tensile properties (modulus of 0.55–0.52 MPa, strain at break of 109–126%), 2) the high ionic conductivity in a solid state and under anhydrous conditions (up to 8.7×10^{-5} S cm^{-1} at 30 °C), 3) the assembly of all-solid-state electrochemical devices such as ionic actuators and piezoionic sensors that show at low scan rates the high volumetric capacitances equivalent or exceeding those reported for the devices with ionic liquids electrolytes. Beyond the reported application, the proposed semi-IPN membranes opened a wide avenue to be the materials of choice for the future development of biomedical devices (as they do not contain any exogenous toxic liquid electrolyte), all-solid-state supercapacitors, electrochromic smart windows, smart textiles, etc.

4. Experimental Section

Materials: Poly(ethylene glycol) methacrylate methyl ether (PEGM, M_w = 500 g mol^{-1}, Sigma-Aldrich), poly(ethylene glycol) dimethacrylate (PEGDM, M_w = 750 g mol^{-1}, Sigma-Aldrich), poly(epichlorohydrin-*co*-ethylene oxide) (Hydrin C2000XL, *m*:*n* = 1:1, $M_w = 8.73 \times 10^6$ g mol^{-1}, M_w/M_n = 4.5 by GPC in THF at 30 °C, Zeon Europe GmbH), lithium bis(trifluoromethanesulfonyl)imide (LiTFSI, 99+%, Solvionic), dicyclohexylperoxidicarbonate (DCPD, 99%, Groupe Arnaud), and poly(3,4-ethylenedioxythiophene):polystyrene sulfonate [PEDOT:PSS] dispersion (Clevios PH1000, solid content 1.0–1.3 wt%, Heraeus GmbH & Co.) were used without further purification. The *N*-methyl imidazole (>99%, Sigma-Aldrich) and *N*-butyl imidazole (98%, Sigma-Aldrich) were distilled over CaH_2.

Synthesis of Poly(1-methyl-3-(oxiran-2-ylmethyl)-1-imidazole-3-ium-co-ethylene oxide) Bis(trifluoromethanesulfonyl)imide (PIL C1): PIL C1 was synthesized via two steps reaction, namely by quaternization reaction of *N*-methyl imidazole by poly(epichlorohydrin-*co*-ethylene oxide) and subsequent ion exchange reaction with LiTFSI in aqueous media. The synthesis was conducting following the procedure published previously[37] although with some minimal changes.

Poly(epichlorohydrin-*co*-ethylene oxide) Hydrin C2000XL (4.00 g, 29,2 mmol) was initially dissolved in 40 mL of anhydrous DMF under inert atmosphere on stirring at 80 °C for 3 h. Afterward 10 equivalents of *N*-methylimidazole (23.97 g, 292.0 mmol) were added in one portion to the polymer solution under inert flow at RT. The temperature was raised to 90 °C and the stirring was continued for 72 h, whereupon the viscous solution was cooled down and precipitated into the excess of acetone. The obtained poly(1-methyl-3-[oxiran-2-ylmethyl]-1-imidazole-3-ium-*co*-ethylene oxide) chloride represented sticky light brown solid. It was thoroughly washed with acetone (3 × 30 mL) and dried at 30 °C/0.1 mbar for 2 h. Yield: 9.3 g (89%); ^{1}H NMR (400.0 MHz, D_2O): δ = 8.78 (s, 1H), 7.54-7.50 (m, 2H), 4.48-4.33 (m, 2H), 3.94 (s, 3H), 3.69-3.62 (m, 7H); ^{13}C NMR (100.6 MHz, D_2O): δ = 136.7, 123.5, 123.2, 76.5, 70.4, 69.6, 50.0, 35.9, 30.3; IR (KBr pellet): 3151 (m), 3102 (w), 2913 (w), 2877 (s, ν_{CH}), 1647 (m), 1570 (m, ν_{CN}), 1456 (m), 1347 (m), 1302 (w), 1252 (w, $\nu_{as-C-O-C-}$), 1165 (s, ν_{-C-O-}), 1088 (vs, $\nu_{s-C-O-C-}$), 952 (w), 874 (w), 843 (w, $\nu_{s-CH2-CO-}$), 746 (m), 700 (w), 635 (m) cm^{-1}.

The solution of lithium bis(trifluoromethylsulfonyl)imide (13.43 g, 45.0 mmol) in 30 mL of milli-Q water was added dropwise to the aqueous solution (100 mL) of poly(1-methyl-3-[oxiran-2-ylmethyl]-1-imidazole-3-ium-*co*-ethylene oxide) chloride (5.12 g, 23.4 mmol) at room temperature. The formation of a precipitate was observed immediately, and the stirring was continued for 2 h at RT. The precipitated sticky product was collected, thoroughly washed with water, redissolved in acetone and reprecipitated in H_2O again. Polymer representing slightly yellow sticky solid was dried at 70 °C /0.1 mbar for 2 days in B-585 oven (Buchi Glass Drying Oven, Switzerland) filled with P_2O_5. Afterward it was transferred under vacuum into the argon filled glove box (MBRAUN MB-Labstar, H_2O and O_2 content < 0.5 ppm) and was stored for 5 days prior to further investigation. Yield: 9.25 g (85%); T_g = –6.2 °C (DSC); T_{onset} = 290 °C (TGA); ^{1}H NMR (400.0 MHz, acetone-d_6): δ = 8.92 (s, 1H), 7.67 (s, 2H), 4.60-4.46 (m, 2H), 4.04 (s, 3H), 3.78-3.64 (m, 6H), 2.91 (s, 1H); ^{13}C NMR (100.6 MHz, acetone-d_6): δ = 138.0, 125.6-116.0 (q, J_{CF} = 321 Hz), 124.3, 77.3, 71.4, 70.9, 69.9, 51.1, 36.6; ^{19}F NMR (376.5 MHz, acetone-d_6): δ = –79.8 (s); IR (ATR-mode): 3159 (w), 3121 (w, ν_{CH}), 2881 (w, ν_{CH}), 1572 (m), 1456 (m), 1354 (vs, ν_{asSO2}), 1195 (vs, ν_{CF}), 1138 (s, ν_{sSO2}), 1058 (vs, ν_{CF}), 842 (w, $\nu_{s-CH2-CO-}$), 741 (m), 618 (s), 571 (s), 512 (m) cm^{-1}.

Synthesis of Poly(1-butyl-3-(oxiran-2-ylmethyl)-1-imidazole-3-ium-co-ethylene oxide) Bis(trifluoromethylsulfonyl)imide (PIL C4): This synthesis followed the same procedure as for PIL C1 described above, although *N*-butyl imidazole was used instead of *N*-methyl imidazole. Yield: 8.93 g (82%); T_g = –25.4 °C (DSC); T_{onset} = 310 °C (TGA); ^{1}H NMR (400.0 MHz, DMSO-d_6): δ = 9.06 (s, 1H), 7.80 (s, 1H), 7.68 (s, 1H), 4.40-4.18 (m, 4H), 4.18-3.81 (m, 2H), 3.81-3.43 (m, 5H), 1.79 (s, 2H), 1.25 (s, 2H), 0.90 (s, 3H); ^{13}C NMR (100.6 MHz, DMSO-d_6): δ = 136.7, 123.4, 122.7-116.3 (q, J_{CF} = 320 Hz), 78.0, 70.1, 69.7, 48.8, 48.6, 44.1, 31.4, 18.7, 13.2; ^{19}F NMR (376.5 MHz, DMSO-d_6): δ = –79.8 (s); IR (KBr pellet): 3113 (w), 2950 (w, ν_{CH}), 2924 (w, ν_{CH}), 2872 (w, ν_{CH}), 1565 (m), 1472 (w), 1349 (vs), 1332 (s, ν_{asSO2}), 1187 (vs, ν_{CF}), 1136 (s, ν_{sSO2}), 1056 (vs, ν_{CF}), 842 (w, $\nu_{s-CH2-CO-}$), 785 (w), 740 (m), 650 (w), 614 (s), 571 (s), 512 (m) cm^{-1}.

Semi-IPN Synthesis: The PEO/PIL C*x* semi-IPNs were synthesized by an in situ method. Regardless the PEO/PIL C*x* ratio, the [PEO+PIL] concentration in cyclohexanone was kept constant at 40 wt%. Similarly, the composition of the PEO network (75 wt% of PEGM and 25 wt% of PEGDM) and the amount of DCPD initiator (3 wt% from the sum of the PEO network precursors (PEGM + PEGDM)) were kept constant as well. An example is provided for the synthesis of 60/40 PEO/PILC4 semi-IPN: PIL C4 (1.00 g) was dissolved in 3.96 mL of cyclohexanone at room temperature for at least 72 h in order to get a homogeneous solution with [PIL C4] concentration of 21 wt%. To the stirred PIL C4 polymer solution the PEGM (0.23 g), PEGDM (0.08 g), and DCPD (0.0093 g, 3 wt% from the sum of methacrylic monomers) were added at room temperature and stirring was continued for 30 min, whereupon the oxygen within the solution was removed by an argon bubbling. In the case of thick films, the resulting solution was then loaded into a mold made from two glass plates clamped together and sealed with a U-shaped Teflon gasket (50.0 mm × 15.0 mm × 0.25 mm). This mold was placed in an oven and kept for 3 h at 50 °C, and finally for 1 h at 80 °C. The resulting film was taken out from the mold and was dried

for 48 h at 80 °C/1 mm Hg with a special flask filled with P_2O_5 and introduced into the vacuum line.

To obtain thin films, the PIL C4/ PEGM /PEGDM /DCPD solution was directly deposited by spin-coating on the suitable substrate which was then heated under dynamic flow of inert gas (argon) for 3 h at 50 °C and additionally for 1 h at 80 °C.

Elaboration of PEDOT:PSS Electrodes: Pristine or neat PEDOT:PSS electrode film was prepared by casting of 70 µL cm^{-2} of a dispersion of PEDOT:PSS on a thoroughly cleaned silicon wafer substrate (typically of 3 × 2 cm^2). The PEDOT:PSS film is obtained by evaporation of water at 30 °C for 2 h under inert gas flow (argon). Thickness 6 µm; $\sigma = 2.6$ S cm^{-1} (25 °C).

[PEDOT:PSS + 45.5 wt% of LiTFSI] electrodes were prepared using the procedure described above, although with addition of LiTFSI (45.5 wt% vs PEDOT:PSS solid content) to the dispersion prior to its casting. The electrode film obtained after drying at 30 °C for 2 h were then thermally annealed at 130 °C for 15 min under inert atmosphere (Ar). Thickness 7.1 µm; $\sigma = 1250$ S cm^{-1} (25 °C).

[PEDOT:PSS + 45.5 wt% of LiTFSI + MeOH-LiTFSI treatment] electrodes were prepared using the procedure described above, although films obtained after drying at 30 °C for 2 h and annealing at 130 °C for 15 min in the inert atmosphere flow were washed thoroughly with the excess of 0.1 g mL^{-1} of LiTFSI solution in methanol. The resultant films were thermally annealed for an extra step at 130 °C for 15 min. Thickness 5.8 µm; $\sigma = 2300$ S cm^{-1} (25 °C).

Trilayer Electroactive Device Assembly: The electroactive trilayers were elaborated following a stacking/polymerization method.[50] In a typical procedure, the bottom electrode was elaborated on a silicon substrate. Then, the cyclohexanone solution containing the precursors of the central semi-IPN membrane was deposited on top of the bottom electrode and spin-coated at 500 rpm for 30 s. The bilayer assembly was then step-wise heated under argon flow for 3 h at 50 °C, 1 h at 80 °C, and for 15 min at 130 °C to conduct the polymerization and thermal post-treatment of the semi-IPN membrane, respectively. On the next step the top electrode was elaborated using the same protocol as for the bottom-one described above. The adhesion by covalent bonds between the different layers was here excluded because electrodes did not contain polymerizable precursors. However, it was assumed that an adhesion between the layers had taken part through other mechanisms such as physical interlacing and/or ionic interactions.[54] The final trilayer device possessed a T-shape with a 2 × 5 mm^2 base for electrical connection, a 6 × 1 mm^2 free-beam shape and a total thickness of 27 µm.

Rheology: Rheological measurements were carried out using an Anton Paar Physica MCR 301 rheometer equipped with a CTD 450 temperature control device with a parallel plate-plate geometry. The solution of semi-IPN precursors were placed directly onto the aluminum plate of the rheometer and measurements were recorded in the oscillation mode at an imposed 1% shear amplitude (γ) for an oscillation frequency of 1 Hz.

Soxhlet Extraction: In order to estimate the amount of unreacted precursors in semi-IPNs and, thus, the efficiency of crosslinking reactions, a known weight of the films was extracted in a Soxhlet apparatus with ethanol for 7 days. After extraction, the samples were dried at 80 °C under dynamic vacuum for 12 h. The extractible content (EC) was given as a weight percentage according to the following Equation (3):

$$\mathrm{EC}\,(\%) = \frac{(W_0 - W_e)}{W_0} \times 100 \tag{3}$$

where W_0 and W_e are the sample weights before and after extraction, respectively.

Dynamic Scanning Calorimetry: DSC measurements were carried out using a Q100 TA (TA Instruments) under a nitrogen flow of 50 mL min^{-1}. Two temperature cycles (heating and cooling) were performed between −85 and +150 °C with 10 °C min^{-1} heating rate. All glass transition temperatures (T_g) were determined during the second heating cycle as the first one was used to eliminate the thermal history of the sample.

Dynamic Mechanical Thermal Analysis: Viscoelastic and mechanical (tensile) studies were performed on a DMTA Q800 (TA Instruments). The viscoelastic behavior of the materials was studied by applying a sinusoidal deformation to a semi-IPN film of known geometry (typically $l \times w \times t = 15 \times 4 \times 0.5$ mm^3). The analysis was conducted in tension mode (deformation of 0.05%; pre-tension of 10^{-3} N), at a load frequency of 1 Hz, between −80 and +150 °C under air and at a heating rate of 3 °C min^{-1}. The set up provided the storage and loss moduli (E' and E'') and the damping parameter or loss factor ($\tan\delta$) defined as the ratio $\tan\delta = E''/E'$. Tensile tests were carried out by monitoring the stress versus strain in air at 25 °C for a tensile speed of 200%/min until the samples break.

Dynamic thermogravimetric analysis (TGA) was performed in air on a Q50 model (TA Instruments) applying a heating rate of 5 °C min^{-1}.

Ionic Conductivity Measurements: All samples prior to measurements were dried for 30 days under dynamic vacuum at 80 °C/1 mm Hg with a special flask filled with P_2O_5 and introduced into the vacuum line. Afterward PILs and semi-IPNs were quickly clamped between two golden electrodes and the ionic conductivity was measured under inert atmosphere with a VSP 150 potentiometer (Biologic) over a frequency range from 300 mHz to 500 KHz. An ac perturbation of 100 mV was applied to the cell. During the tests, the temperature was controlled by means of programmable hot gold electrodes. The conductivity value was calculated from the bulk resistance in the complex impedance diagram according to the following Equation (4):

$$\sigma\left(cm^{-1}\right) = \frac{e}{Z \times S} \tag{4}$$

where e (cm) is the thickness of the sample, S (cm^2) is its surface, and Z is the real part of the complex impedance.

Water Content: The water content of semi-RIP materials was measured using a Karl–Fischer Titrator Thermoprep 860 (Metrohm). The measurement of the residual water content by Karl–Fisher method highlighted that 2 wt% of water still remained in the samples even after the prolonged drying process (Figure S10, Supporting Information).

Electroactive Device Characterizations: The electromechanical (actuator) and mechanoelectrical (sensor) performances of the electroactive trilayers were studied with a potentiostat (Biologic VSP 150) in a two-electrode system configuration. The sample were cut into strips with a length of 6 mm, width of 1 mm and a total thickness of ≈30 µm. The bending deformation in actuator mode was determined by applying square wave potential (±1.75 V) between the two electrodes of the trilayer and by following the resulting bending displacement over time with a laser displacement sensor LKG 32 (Keyence) (distance of measurement : 3 mm vs the clamped position of the beam). In order to normalize the values, the resulting strain difference $\Delta\varepsilon$ between the two PEDOT:PSS electrodes was calculated according to Sugino et al.,[51] where D is the displacement of the actuator from neutral to actuated state, h is the thickness of the actuator, and L_0 is the distance between the clamped end of the actuator and the laser beam.

$$\Delta\varepsilon = \frac{2Dh}{\left(L_0^2 + D^2\right)} \tag{5}$$

The mechanical sensing performances of the trilayers were measured by applying a controlled bending deformation to the beam thanks to a microrobotic system FT-RS1002 (Femtotools) with a microforce sensing probe FT-S1000 (Femtotools) and by measuring the corresponding open circuit voltage (OCV) variation.

Statistical Analysis: Each measurement was performed on one to three samples for each series of composition. The mean deviation on T_g onset had been evaluated at 3 °C, the mean deviation on the conductivity onset had been evaluated at 20%, the mean error of extractible content at 2%, the mean error on the Young's modulus at 10%, and the mean error on electronic conductivity at 10%. All data were extracted, analyzed, and plotted with MS Excel, Origin 8, and Origin 2022.

Supporting Information

Supporting Information is available from the Wiley Online Library or from the author.

Acknowledgements

This work was supported by the French "Agence Nationale pour la Recherche (ANR)" in part through Micro-TIP project (Microsystem including transducers based interpenetrating networks, ANR-15-CE08-0032), in part by the Luxembourg National Research Fund (FNR) and Fonds de la Recherche Scientifique (F.R.S.-FNRS) through FNRS-FNR project INFINITE (Agreement number INTER/FNRS/21/16555380/INFINITE), and in part by European Union's Horizon 2020 research and innovation program through WEAFING project (Wearable Electroactive Fabrics Integrated in Garments, Grant agreement ID: 825232). Zeon Europe GmbH (Halle, Germany) is acknowledged for supplying of Hydrin C2000XL epichlorohydrin/ethylene oxide copolymer free of charge.

Conflict of Interest

The authors declare no conflict of interest.

Data Availability Statement

The data that support the findings of this study are available in the Supporting Information of this article.

Keywords

all-solid-state electrolytes, flexible electroactive devices, interpenetrating polymer networks, ionic actuators, piezoionic sensors, polymeric ionic liquids

Received: November 18, 2022
Revised: January 11, 2023
Published online: March 3, 2023

[1] L. Hines, K. Petersen, G. Z. Lum, M. Sitti, *Adv. Mater.* **2017**, *29*, 1603483.
[2] H. Kim, K. R. Pyun, M. T. Lee, H. B. Lee, S. H. Ko, *Adv. Funct. Mater.* **2022**, *32*, 2110535.
[3] C. Yang, Z. Suo, *Nat. Rev. Mater.* **2018**, *3*, 125.
[4] K. Xiao, C. Wan, L. Jiang, X. Chen, M. Antonietti, *Adv. Mater.* **2020**, *32*, 2000218.
[5] H. J. Kim, B. Chen, Z. Suo, R. C. Hayward, *Science* **2020**, *776*, 773.
[6] X. Ming, C. Zhang, J. Cai, H. Zhu, Q. Zhang, S. Zhu, *ACS Appl. Mater. Interfaces* **2021**, *13*, 31102.
[7] D. Mecerreyes, *Prog. Polym. Sci.* **2011**, *36*, 1629.
[8] A. Eftekhari, T. Saito, *Eur. Polym. J.* **2017**, *90*, 245.
[9] G. A. Tiruye, D. Muñoz-Torrero, J. Palma, M. Anderson, R. Marcilla, *J. Power Sources* **2015**, *279*, 472.
[10] P. S. C. de Oliveira, S. A. Alexandre, G. G. Silva, J. P. C. Trigueiro, R. L. Lavall, *Eur. Polym. J.* **2018**, *108*, 452.
[11] G. G. Eshetu, D. Mecerreyes, M. Forsyth, H. Zhang, M. Armand, *Mol. Syst. Des. Eng.* **2019**, *4*, 294.
[12] E. I. Lozinskaya, D. O. Ponkratov, I. A. Malyshkina, P. Grysan, G. Lingua, C. Gerbaldi, A. S. Shaplov, Y. S. Vygodskii, *Electrochim. Acta* **2022**, *413*, 140126.
[13] N. A. Rice, W. J. Bodnaryk, B. Mirka, O. A. Melville, A. Adronov, B. H. Lessard, *Adv. Electron. Mater.* **2019**, *5*, 1800539.
[14] M. N. Tousignant, M. Ourabi, J. Niskanen, B. Mirka, W. J. Bodnaryk, A. Adronov, B. H. Lessard, *Flexible Printed Electron.* **2022**, *7*, 034004.
[15] C.-P. Lee, K.-C. Ho, *Eur. Polym. J.* **2018**, *108*, 420.
[16] C. Shen, Q. Zhao, C. M. Evans, *Adv. Mater. Technol.* **2019**, *4*, 1.
[17] F. B. Ribeiro, C. Plesse, G. T. M. Nguyen, S. M. Morozova, E. Drockenmuller, A. S. Shaplov, F. Vidal, in Proceedings SPIE - Electroactive Polymer Actuators and Devices, SPIE, Denver, CO **2018**, p. 10594.
[18] W. Qian, J. Texter, F. Yan, *Chem. Soc. Rev.* **2017**, *46*, 1124.
[19] A. S. Shaplov, D. O. Ponkratov, P. S. Vlasov, E. I. Lozinskaya, L. I. Komarova, I. A. Malyshkina, F. Vidal, G. T. M. Nguyen, M. Armand, C. Wandrey, Y. S. S. Vygodskii, *Polym. Sci., Ser. B* **2013**, *55*, 122.
[20] V. Ganesan, *Mol. Syst. Des. Eng.* **2019**, *4*, 280.
[21] S. Tsuzuki, H. Tokuda, K. Hayamizu, M. Watanabe, *J. Phys. Chem. B* **2005**, *109*, 16474.
[22] S. Tsuzuki, *ChemPhysChem* **2012**, *13*, 1664.
[23] H. Ohno, M. Yoshizawa, W. Ogihara, *Electrochim. Acta* **2004**, *50*, 255.
[24] S. Washiro, M. Yoshizawa, H. Nakajima, H. Ohno, *Polymer* **2004**, *45*, 1577.
[25] L. Porcarelli, P. S. Vlasov, D. O. Ponkratov, E. I. Lozinskaya, D. Y. Antonov, J. R. Nair, C. Gerbaldi, D. Mecerreyes, A. S. Shaplov, *Eur. Polym. J.* **2018**, *107*, 218.
[26] A. S. Shaplov, R. Marcilla, D. Mecerreyes, *Electrochim. Acta* **2015**, *175*, 18.
[27] L. Porcarelli, A. S. Shaplov, M. Salsamendi, J. R. Nair, Y. S. Vygodskii, D. Mecerreyes, C. Gerbaldi, *ACS Appl. Mater. Interfaces* **2016**, *8*, 10350.
[28] A. Vollas, T. Chouliaras, V. Deimede, T. Ioannides, J. Kallitsis, *Polymers* **2018**, *10* ,912
[29] N. A. Agudelo, A. M. Elsen, H. He, B. L. López, K. Matyjaszewski, *J. Polym. Sci., Part A: Polym. Chem.* **2015**, *53*, 228.
[30] H. Mori, M. Yahagi, T. Endo, *Macromolecules* **2009**, *42*, 8082.
[31] L. H. Sperling, *Interpenetrating Polymer Networks and Related Materials*, Springer US, New York **1981**.
[32] F. Vidal, C. Plesse, G. Palaprat, A. Kheddar, J. Citerin, D. Teyssié, C. Chevrot, *Synth. Met.* **2006**, *156*, 1299.
[33] A. S. Shaplov, D. O. Ponkratov, P. S. Vlasov, E. I. Lozinskaya, L. V. Gumileva, C. Surcin, M. Morcrette, M. Armand, P.-H. Aubert, F. Vidal, Y. S. Vygodskii, *J. Mater. Chem.* **2015**, *3*, 2188.
[34] J. Juger, C. Vancaeyzeele, C. Plesse, G. M. T. Nguyen, F. B. Ribeiro, D. Teyssié, F. Vidal, *Eur. Polym. J.* **2018**, *106*, 257.
[35] A. S. Shaplov, D. O. Ponkratov, P. S. Vlasov, E. I. Lozinskaya, I. A. Malyshkina, F. Vidal, P.-H. Aubert, M. Armand, Y. S. Vygodskii, *Polym. Sci., Ser. B* **2014**, *56*, 164.
[36] A. S. Shaplov, L. Goujon, F. Vidal, E. I. Lozinskaya, F. Meyer, I. A. Malyshkina, C. Chevrot, D. Teyssie, I. L. Odinets, Y. S. Vygodskii, *J. Polym. Sci., Part A: Polym. Chem.* **2009**, *47*, 4245.
[37] D. O. Ponkratov, E. I. Lozinskaya, P. S. Vlasov, P.-H. H. Aubert, C. Plesse, F. Vidal, Y. S. Vygodskii, A. S. Shaplov, *Electrochim. Acta* **2018**, *281*, 777.
[38] T. Ikeda, S. Moriyama, J. Kim, *J. Polym. Sci., Part A: Polym. Chem.* **2016**, *54*, 2896.
[39] A. S. Shaplov, E. I. Lozinskaya, D. O. Ponkratov, I. A. Malyshkina, F. Vidal, P. H. Aubert, O. V. Okatova, G. M. Pavlov, L. I. Komarova, C. Wandrey, Y. S. Vygodskii, *Electrochim. Acta* **2011**, *57*, 74.
[40] M. A. Ratner, P. Johansson, D. F. Shriver, *MRS Bull.* **2000**, *25*, 31.
[41] P. Verge, M. Mallouki, L. Beouch, P. H. Aubert, F. Vidal, F. Tran-Van, D. Teyssié, C. Chevrot, *Mol. Cryst. Liq. Cryst.* **2010**, *522*, 53/[353].

[42] A. Papagiannopoulos, E. Vlassi, S. Pispas, C. Tsitsilianis, A. Radulescu, *Macromol* **2021**, *1*, 37.
[43] I. M. Kalogeras, in *Encyclopedia of Polymer Blends*, Wiley, Hoboken, NJ **2016**, Ch. 1.
[44] F. Liu, Y. Lv, J. Liu, Z. C. Yan, B. Zhang, J. Zhang, J. He, C. Y. Liu, *Macromolecules* **2016**, *49*, 6106.
[45] L. H. Sperling, V. Mishra, *Polym. Adv. Technol.* **1996**, *7*, 197.
[46] S. H. Eom, S. Senthilarasu, P. Uthirakumar, S. C. Yoon, J. Lim, C. Lee, H. S. Lim, J. Lee, S.-H. Lee, *Org. Electron.* **2009**, *10*, 536.
[47] F. Zabihi, Y. Xie, S. Gao, M. Eslamian, *Appl. Surf. Sci.* **2015**, *338*, 163.
[48] E. Dauzon, Y. Lin, H. Faber, E. Yengel, X. Sallenave, C. Plesse, F. Goubard, A. Amassian, T. D. Anthopoulos, *Adv. Funct. Mater.* **2020**, *30*, 2001251.
[49] Y. Wang, C. Zhu, R. Pfattner, H. Yan, L. Jin, S. Chen, F. Molina-Lopez, F. Lissel, J. Liu, N. I. Rabiah, Z. Chen, J. W. Chung, C. Linder, M. F. Toney, B. Murmann, Z. Bao, *Sci. Adv.* **2017**, *3*, 1.
[50] K. Rohtlaid, G. T. M. Nguyen, C. Soyer, E. Cattan, F. Vidal, C. Plesse, *Adv. Electron. Mater.* **2019**, *5*, 1800948.
[51] T. Sugino, K. Kiyohara, I. Takeuchi, K. Mukai, K. Asaka, *Sens. Actuators, B* **2009**, *141*, 179.
[52] J. D. Madden, P. G. Madden, I. W. Hunter, in Smart Structures and Materials 2001: Electroactive Polymer Actuators and Devices, SPIE, Newport Beach, CA **2001**, pp. 72–83.
[53] Y. I. S. Z. Bisri, S. Shimizu, M. Nakano, *Adv. Mater.* **2017**, *29*, 1607054.
[54] X. Jin, L. Heepe, J. Strueben, R. Adelung, S. N. Gorb, A. Staubitz, *Macromol. Rapid Commun.* **2014**, *35*, 1551.